Formation and Optimization of Vein Networks in *Physarum*

Rodrigo Almeida

Under supervision of *Prof. Rui Dilão*

Department of Physics and Nonlinear Dynamics Group, Instituto Superior Técnico, Lisboa, Portugal

(Dated: July 2021)

We construct a flow-based model for the adaptive network formation of *Physarum*, which solves some inconsistencies of previous models. We first derive a general class of equations describing the adaptation and flow dynamics of a static network comprised of elastic channels filled with an incompressible fluid undergoing a Hagen-Poiseuille flow. An explicit form of the model is obtained by minimising the total power dissipated by the network. Considering a more general functional form of the adaptive equations a phase transition in the system is also found. The model is used to build efficient and resilient networks in an arena mimicking mainland Portugal by considering fluctuating loads. Finally, the adaption model is extended to incorporate the network growth in the presence of multiple food sources. The coupling of both processes produces networks with similar traits to several network systems found in nature. We found that when the food sources operate alternately, the model can replicate the direct connections between the food sources observed in *Physarum*.

Keywords: *Physarum polycephalum*, Adaptive network, Network optimisation, Network formation, Hagen-Poiseuille

I. INTRODUCTION

Recently, attention has focused on the acellular slime mould, *Physarum polycephalum*, as an ideal model organism to study the interplay between structure and function in biological transport networks, and to understand the mechanism underlying several complex behaviours displayed by simple organisms, such as the adaptive network formation. *Physarum* is a single-celled amoeboid organism that grows as an extensive and highly adaptive network of veins filled with endoplasmic fluid. As it forages and progressively accommodates new food sources, *Physarum* dynamically optimises the connections between them, by adapting the thickness of the network veins. The adaptation is believed to be related to local changes in the flux flow, driven by rhythmical contractions of the vein walls whose frequency and amplitude are regulated by food sources and other external stimuli [1]. Despite lacking any kind of neural circuit, *Physarum* displays high-level behaviours, arising from the network adaptation. For instance, it can solve mazes [2], and in the presence of multiple food sources, it can build networks with a trade-off between total length, transport efficiency and fault tolerance, comparable to real human-made networks [3].

Different flow-based models have been proposed to describe the network optimisation of *Physarum*. These models describe the organism as a Hagen-Poiseuille flow network with adaptive channel conductivities. The optimisation is described by *ad hoc* local evolution laws for the conductivities based on the current-reinforcement principle [3, 4], where the flow modifies the network architecture, which in turn affects the flows. However, these models violate some basic physical principles, such as the conservation of volume of the circulating fluid, as assumed by a Hagen-Poiseuille flow. Furthermore, in general, they don't incorporate network growth.

The goal of this work is to build a generic model for the network formation and optimisation as observed during the growth of *Physarum polycephalum* that addresses these two issues.

II. MODEL FORMULATION

The geometry of *Physarum*'s vein network is described as an undirected, planar and connected graph, $\mathcal{G} = (V, E)$, embedded in the Euclidean plane, where V is the set of N nodes with coordinates (x_i, y_i) for $i \in V$, and E is the set of M straight edges (i, j), connecting the node i and j. The edges represent the network veins (channels), and the nodes the junctions between them.

Each node i is characterised by a pressure p_i. An edge (i, j) is assumed to be a cylindrical elastic channel with a fixed length L_{ij}, and a radius r_{ij} which can change in response to the magnitude of flux $|Q_{ij}|$ flowing through it. The fluid in the network is viscous and incompressible, and undergoes a Hagen-Poiseuille flow, being the channels fluxes Q_{ij} given by

$$Q_{ij} = \frac{\pi r_{ij}^4 (p_i - p_j)}{8\eta L_{ij}} = \frac{D_{ij}(p_i - p_j)}{L_{ij}} \quad (1)$$

where D_{ij} is the conductivity of the channel (i, j), and $D_{ij} = D_{ji}$. If $Q_{ij} > 0$, then the fluid flows from i to j, while $Q_{ij} < 0$ means that the flow is from j to i. The ratios D_{ij}/L_{ij} can be seen as edge-weights.

The volume of a channel (i, j) is $\mathcal{V}_{ij} = \pi r_{ij}^2 L_{ij}$. As $D_{ij} = \pi r_{ij}^4/8\eta$, we have $\mathcal{V}_{ij} = \sqrt{8\pi\eta} L_{ij} \sqrt{D_{ij}}$. As the fluid is incompressible, the volume of fluid in the network is constant and is

$$\mathcal{V} = \sum_{(i,j)\in E} \mathcal{V}_{ij} = \beta \sum_{(i,j)\in E} L_{ij}\sqrt{D_{ij}}, \qquad (2)$$

where $\beta = \sqrt{8\pi\eta}$. We assume that the network flows are driven by a set of sources and sinks (terminals), located at fixed nodes, which mimic stimulated regions of *Physarum*. Each node i is thus characterised by a net flux q_i. If a node i is a source, it injects flux in the system, and $q_i > 0$. If the node is a sink, it removes flows from the system, and $q_i < 0$; otherwise $q_i = 0$. The volume conservation of the fluid imposes that

$$\sum_{i\in V} q_i = \sum_{i\in\text{sources}} q_i + \sum_{i\in\text{sinks}} q_i = 0 . \qquad (3)$$

The channel flux can be determined by the conservation of the flux at each vertex i

$$\sum_{j\in\mathcal{N}(i)} Q_{ij} = q_i \quad , \quad i \in V , \qquad (4)$$

where $\mathcal{N}(i) = \{j : (i,j) \in E\}$ is the set of the neighbour nodes of the node i.

Regarding the adaptation dynamics of the network, we assume that the area of channels, $\pi r_{ij}^2 \propto \sqrt{D_{ij}}$, can change in response to the fluxes, and make the *ansatz*

$$\frac{d}{dt}\sqrt{D_{ij}} = f(|\mathbf{Q}|) - \mu\sqrt{D_{ij}} , \qquad (5)$$

where $f(\mathbf{Q})$ is an unknown function of all the network fluxes $\mathbf{Q}$, with $f(\mathbf{0}) = 0$, which generically describes the channel expansion due to the flux. The second term represents the tube shrinkage at a rate $\mu > 0$ in the absence of flux. Below, we discuss the consistency of the *ansatz*.

By differentiating both sides of (2), the conservation of the volume can be described by the following constraint

$$\frac{d\mathcal{V}}{dt} = \beta \sum_{(i,j)\in E} L_{ij}\frac{d}{dt}\sqrt{D_{ij}} = 0 . \qquad (6)$$

Replacing (5) in the last equation and using (2) implies that

$$\sum_{(i,j)\in E} L_{ij}f(|\mathbf{Q}|) = \mu \sum_{(i,j)\in E} L_{ij}\sqrt{D_{ij}} = \mu\frac{\mathcal{V}}{\beta} \qquad (7)$$

is constant. In order to satisfy this condition, it's sufficient to define f in terms of a new function g by the relation

$$f(|\mathbf{Q}|) := \frac{\mu}{\beta}\mathcal{V}\frac{g(|Q_{ij}|)}{\sum_{(k,m)\in E} L_{km}g(|Q_{km}|)} . \qquad (8)$$

By introducing the last expression into the *ansatz* (5), and redefining the time scale $\tau = \mu t$ we obtain

$$\frac{d}{d\tau}\sqrt{D_{ij}} = \frac{\mathcal{V}}{\beta}\frac{g_{ij}}{\sum_{(k,m)\in E} L_{km}g_{km}} - \sqrt{D_{ij}} \quad , \quad (i,j) \in E \qquad (9)$$

where $g_{ij} \equiv g(|Q_{ij}|)$. Therefore, we conclude that for any choice of the function g, the volume of the fluid in a network with adaptive channels' conductivities evolving according to (9) is conserved over time. Thus, it may correctly describe the adaptation of a Hagen-Poiseuille flow network. Note that the adaptation rule (9) depends on the global structure of the flows through the term $Z \equiv \sum_{(k,m)} L_{km}g(|Q_{km}|)$, making the adaptation explicitly a non-local process, in contrast to previous models [3] where the coupling of the system's dynamics stems only from conservation of the flux at the nodes (4).

III. MINIMISATION OF ENERGY DISSIPATION

In order to analyse the temporal evolution of a network following the adaptation dynamics (9), the function g must be chosen. Here, the choice of g is made by introducing the criterion of minimisation of the total power dissipated during the flow (dissipation), subject to the constraint of the fixed volume of fluid and assuming a steady flow imposed by a fixed set of sources and sinks [5].

When a viscous fluid flows through a channel, some energy is lost due to friction. The total power dissipated by a Hagen-Poiseuille flow network is

$$\mathcal{P} = \sum_{(i,j)\in E} \Delta p_{ij}Q_{ij} = \sum_{(i,j)\in E} \frac{Q_{ij}^2}{D_{ij}}L_{ij} . \qquad (10)$$

We seek to minimise the dissipation rate, $\mathcal{P}$, of a steady flow network with respect to $\sqrt{D_{ij}}$ with $(i,j) \in E$, subject to the local constraints of flux conservation (4), and the additional global constraint of a constant volume, $\mathcal{V}$ (incompressible fluid). The problem consists of minimising the following Lagrangian

$$\mathcal{L} = \mathcal{P} - \lambda(\mathcal{V} - \beta \sum_{(k,m)\in E} \sqrt{D_{km}}L_{km}) \qquad (11)$$

where λ is a Lagrangian multiplier. The set of conductivities that minimises $\mathcal{L}$ is the solution of

$$\begin{cases} \dfrac{\partial \mathcal{L}}{\partial \sqrt{D_{ij}}} = \left(-\dfrac{Q_{ij}^2}{D_{ij}^2} L_{ij} + 2 \sum_{(k,m) \in E} \dfrac{Q_{km}}{D_{km}} \dfrac{\partial Q_{km}}{\partial D_{ij}} L_{km} \right. \\ \qquad\qquad \left. + \lambda \beta \dfrac{L_{ij}}{2\sqrt{D_{ij}}} \right) 2\sqrt{D_{ij}} = 0 \\ \dfrac{\partial \mathcal{L}}{\partial \lambda} = \mathcal{V} - \beta \sum_{(k,m) \in E} L_{km} \sqrt{D_{km}} = 0. \end{cases}$$

If we assume time-independent sources and sinks, one can show that the second term on the right-hand side of the first equation is zero (cf. Lemma 2.1 in [6]). Solving these equations with respect to D_{ij} and λ, we find that the non-trivial values of conductivities that minimise the total dissipation of the network flow are

$$D_{ij} = \left(\frac{\mathcal{V}}{\beta} \frac{Q_{ij}^{2/3}}{\sum\limits_{(k,m) \in E} Q_{km}^{2/3} L_{km}} \right)^2 . \qquad (12)$$

On the other hand, we find that the non-trivial steady states of the volume-preserving adaptation law (9) satisfy

$$\frac{d}{d\tau} \sqrt{D_{ij}^*} = 0 \quad \Leftrightarrow \quad D_{ij}^* = \left(\frac{\mathcal{V}}{\beta} \frac{g_{ij}}{\sum\limits_{(k,m) \in E} L_{km} g_{km}} \right)^2 . \qquad (13)$$

Comparing (12) with (13), we conclude that for the choice of $g_{ij} = Q_{ij}^{2/3}$, the total dissipation of the network at the steady state is minimal, assuming a constant distribution of nodes flux, $\boldsymbol{q}$, during the adaptation process. This specific choice led us to consider the more general class of polynomial functions, $g_\gamma(|Q_{ij}|) := |Q_{ij}|^\gamma$, where $\gamma > 0$ is a new parameter, and the absolute value in Q_{ij} emphasises that conductivities are independent of the flow direction. In the following, we analyse the evolution of the system subject to the adaptation dynamics

$$\frac{d}{d\tau} \sqrt{D_{ij}} = \frac{\mathcal{V}}{\beta} \frac{|Q_{ij}|^\gamma}{\sum\limits_{(k,m) \in E} L_{km} |Q_{km}|^\gamma} - \sqrt{D_{ij}} \qquad (14)$$

as a function of the parameter γ.

As a side note, for the simplest case of a single elastic channel with length L_{12} and conductivity D_{12}, the equation (9) reduces to $\frac{d}{d\tau} \sqrt{D_{12}} = \mathcal{V}/(\beta L_{12}) - \sqrt{D_{12}}$, which has a unique stable fixed point for $\sqrt{D_{12}^*} = \mathcal{V}/(\beta L_{12})$, coinciding with (12). Therefore, according to our model (9), for a Hagen-Poiseuille flow on a single elastic tube, the radius of the tube at the steady state minimises the power dissipated by the flow, regardless of the choice of g. This property is consistent with the distribution of

channel fluxes arising from the Kirchhoff Law (4), which is by definition the one which minimises the total power dissipated [7], and thus justifies the *ansatz* made in (5) by adding the term $\sqrt{D_{ij}}$.

IV. METHODS

A. Algorithm

The algorithm used to simulate our model is described in the following. First, we generate a planar graph, $\mathcal{G}$, embedded in the two-dimensional Euclidean space, which represents the initial geometry of *Physarum*'s network. The edge lengths L_{ij} are obtained based on the nodes' positions. These two remain fixed throughout the simulation, and only the conductivities, D_{ij} are the target of the adaptation. Some of the nodes are assigned as sources or sinks and have a net flux different from zero, such that the constraint (3) is verified. The initial conditions of our dynamical system are the initial edges conductivities, $D_{ij}(0)$. Usually, we consider an initial homogeneous distribution, and if they aren't specified, it's assumed $D_{ij}(0) = 1$ for all edges $(i, j) \in E$. The initial conductivities are used to compute the total volume of fluid through (2), where we always consider the parameter $\beta = 1$.

Given the distribution of nodes' net fluxes, $\boldsymbol{q}$, and the initial set of edge conductivities, the temporal evolution of the system starts with the computation of the channel fluxes, Q_{ij} by solving the linear system (4). Then, based on those fluxes, the conductivities of all the channels are updated according to (14), or more generally, according to (9) given a predefined function g. The new channel conductivities are used to compute the new channel fluxes in the next time step of the algorithm. These steps are repeated over time until a steady state of channel conductivities is eventually reached. From the numerical point of view, we consider that a steady state is reached when the condition $\max\limits_{(i,j) \in E} |D_{ij}(n\Delta\tau) - D_{ij}((n-1)\Delta\tau)| \leq 10^{-6}$ is verified, where n is the first integer for which the inequality is verified, and $\Delta\tau$ is the time increment used to solve numerically the adaptation rule (9). The time of convergence of the adaptation algorithm is thus $\tau* = n\Delta\tau < \infty$.

The geometry of the initial networks was generated through a Delaunay Triangulation of a set of points representing the nodes, in order to avoid the influence of lattice symmetries in the results.

B. Computation of the network flows

The channel fluxes in each time step are computed by first finding the pressures of the nodes. If we define $\mathbf{p}$ and $\mathbf{q}$ as the N-dimensional vectors whose ith elements are respectively the pressure p_i and the net current q_i of

the ith node, then the linear system (4) can be rewritten in the matrix form as $\boldsymbol{L}\mathbf{p} = \mathbf{q}$, where $\boldsymbol{L}$ is a $N \times N$ symmetric matrix with entries

$$\ell_{ij} = \left(\sum_k C_{ik}\right)\delta_{ij} - C_{ij} , \qquad (15)$$

with $C_{ij} = D_{ij}/L_{ij}$. Finally, once the pressures of the nodes are determined, the channel fluxes can be computed through (1).

C. Numerical Scheme

In this work, we adopt a simple explicit Euler numerical scheme with a time step $\Delta\tau$, which results in the following discretisation of (9)

$$\sqrt{D_{ij}^{n+1}} = \sqrt{D_{ij}^n} + \Delta\tau\left(\frac{\mathcal{V}}{\beta}\frac{g_{ij}^n}{\sum_{(k,m)\in E}L_{km}g_{km}^n} - \sqrt{D_{ij}^n}\right) ,$$
$$(16)$$

where D_{ij}^n denotes the conductivity of the edge (i,j) at the time $\tau = n\Delta\tau$, i.e $D_{ij}^n \equiv D_{ij}(n\Delta\tau)$ and similarly $g_{ij}^n \equiv g(|Q_{ij}(n\Delta\tau)|)$. It's straightforward to show that the Euler method conserves the volume of the channels from one step to another, as required.

Most of the simulations were carried out with relatively a large time increment, $\Delta\tau = 0.1$, due to computation power limitations.

V. EXPLORATION OF THE MODEL

We started by performing simple tests on the model. In this work we adopt the following conventions: the sources are represented by yellow circles, the sinks are represented by red triangles, and the thickness of the lines representing the edges is proportional to their radius ($D_{ij}^{1/4}$). The initial network is also shown in light red.

A. Network temporal evolution

In Figure,1 we've simulated the adaptive mechanism on a setting mimicking the *Physarum* scenario. We've considered an an organism with a circular shape in the presence of a central food source which acts as a source of nutrients flux with intensity $q_{source} = 1$. The nutrients are equally distributed between all the nodes at the boundary, which behave like sinks, simulating regions where there is a continuous nutrient uptake so that the eventual growth of the organism may occur (which is neglected for now).

The final network shows a preferential radial orientation consistent with the flux direction and resembles in some degree the networks displayed by *Physarum*. However, the key difference is that *Physarum* networks have some redundancy and hierarchy of veins, which is not observed in the simulations.

In all the simulations, the adaptation dynamics (14) for $\gamma = 2/3$ resulted in steady-state networks which looked like *trees*, *i.e.* acyclic connected graphs where any two vertices are connected by exactly one path. This is partly due to assuming fixed sources and sinks, and thus neglecting flux fluctuations that are believed to be important for the formation of those redundant paths [8, 9]. The impact of the flux fluctuations will be explored later.

B. Initial Conditions

We have studied the uniqueness of the steady state solutions of dynamics (14) for $\gamma = 2/3$. Considering the same configuration, we simulated the dynamics starting from tested different sets of initial conductivities, draw each time from a uniform distribution in the interval [0,2], *i.e.* $D_{ij}(0) \sim U(0,2)$. Figure 2 shows the steady-state networks of two simulations on a configuration of 3 sources and 5 sinks. We can conclude that for a given setting the system may have multiple steady-state solutions, as one could have expected.

One can also show that the adaptive equations (14) are invariant under scaling transformations of the initial conductivities. This implies that if the latter are scaled by a global factor, the conductivities of the steady state are also scaled by the same factor, but the topology of the steady-state graph remains the same. This was confirmed by numerous simulations.

C. Phase Transition

Considering the same *Physarum* scenario of the simulation in Figure 1, we have simulated the dynamics (14) for different values of $\gamma \in [0,2]$ starting from random initial conductivities, $D_{ij}(0) \sim U(1/2, 3/2)$. Two examples of the steady-state networks reached by the system for different values of γ are shown in Figure 3.

Extensive simulations revealed a drastic change in the topology of the steady-states for $\gamma = 1/2$, the existence of a phase transition in the system. For $\gamma < 1/2$, the steady-state networks have many loops and channels with similar radius. By contrast, for $\gamma > 1/2$ no loops remain, and the steady states are *trees* spanned by the central source and the boundary sinks, with a clear hierarchy of veins thickness. However, once more we haven't found networks with a reticulated hierarchic structure for any value of γ, as observed in the real networks produced by *Physarum*.

The phase transition at $\gamma \simeq 1/2$ was quantified through the evaluation of different network metrics at the

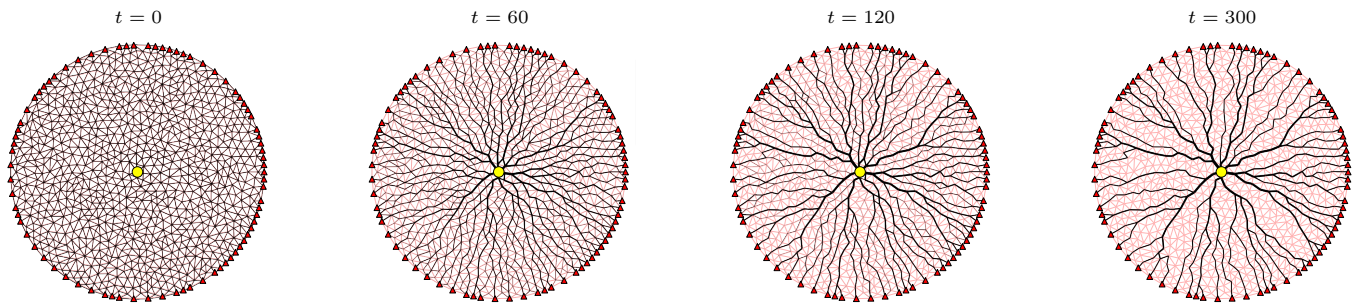| $t = 0$ | $t = 60$ | $t = 120$ | $t = 300$ |

FIG. 1: Snapshots of a simulation replicating *Physarum*'s network adaptation for $\gamma = 2/3$. The flux is driven by a central source (yellow) and the sinks (red) placed at the boundary of the organism, which represents stimulated regions with high metabolic activity. The source gives $q_{source} = 1$, which is evenly distributed between the sinks.
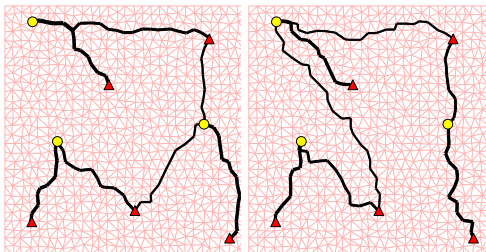

FIG. 2: Dependence of the steady states' topology on the initial conductivities ($q_{source} = 1/3$, $q_{sink} = -1/5$, $\gamma = 2/3$). Each steady state was obtained by considering a different random set of initial conductivities, $D_{ij}(0) \sim U(0, 2)$.
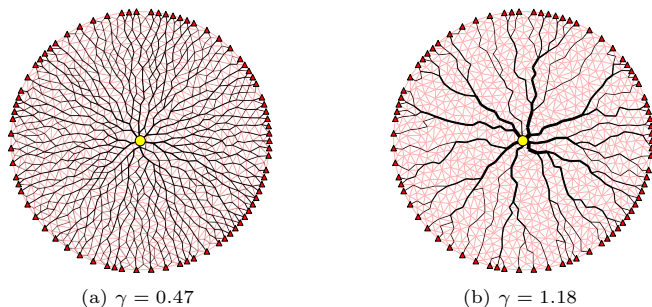

(a) $\gamma = 0.47$ (b) $\gamma = 1.18$

FIG. 3: Dependency of the steady states of the dynamics (14) on γ, for the same configuration of Figure 1.

steady-state of each γ. The first two are the total power dissipated by the network (10) and its total length, L.

Finally, we have considered the loop density [8], LD, as a simple measure of the network's redundancy, defined as the number of independent loops of the steady-state network, normalised by that of the initial network , which in our case, corresponds to the number of triangles of the initial Delaunay triangulation. Since the networks are connected and planar, the number of loops or faces, f, can be determined using Euler's formula $f = 1 + M - N$, where $M = |E|$ is the number of edges, and $N = |V|$ the number of vertices.

Note that only edges with conductivities above a threshold ($D_{thr} = 5 \times 10^{-4}$) were considered in the computation of the total length and the number of loops of the final

networks.

The dependency of these quantities on γ is plotted in Figure 4. The change in the slope of the network dissipation, $\mathcal{P}(\gamma)$, observed at $\gamma = 1/2$, suggests the existence of a discontinuity on its first derivative with respect to γ, which may correspond to a first-order phase transition, according to the Ehrenfest classification.

Contrary to expectations, Figure 4b shows that the minimum of $\mathcal{P}(\gamma)$ is not reached for $\gamma = 2/3$, as derived in (12). This is most likely due to the large contributions of the channels with very low conductivities and fluxes to the uncertainty of the power dissipated, which are added from one step to another. Other configurations of terminals were also tested, and in most cases, the minimum was indeed reached at $\gamma = 2/3$.

The transition is even more clear in the plots of total length (Figure 4c) and loop density (Figure 4d). In particular, the absence of loops for $\gamma > 1/2$, confirms that the steady-states are *trees*, assuming the threshold $D_{thr} = 5 \times 10^{-4}$. Further simulations revealed that the phase transition is independent of the initial distribution of conductivities and of the configuration of terminals.

VI.   APPROXIMATING PORTUGAL'S RAILWAY SYSTEM

The design of an optimal network requires a complex trade-off between the production cost, transport efficiency and fault tolerance. As the Tokyo experiments [3] showed, *Physarum* produce networks with a good compromise between these three metrics, and comparable to those of real-world infrastructure network, in particular, to the Tokyo railway system.

Inspired by those experiments, we have simulated the adaptation dynamics (14) for different values of γ considering a mesh with the shape of mainland Portugal. We have considered a configuration of 25 terminals, representing the geographical locations of the 18 Portuguese district capitals and 7 additional major cities, except for the Viseu district which was represented by the city Mangualde for convenience. The resulting networks were compared with the section of the Portuguese rail network
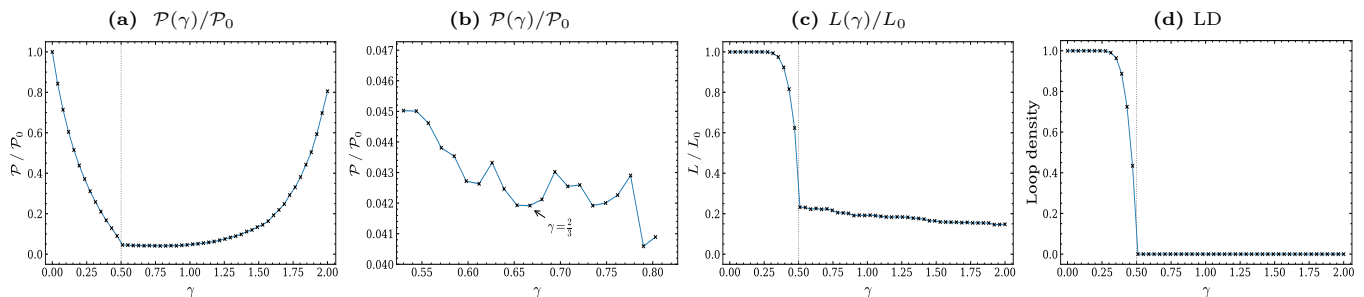
FIG. 4: Plots of different metrics of the steady-state networks, as function of γ. **(a)** Network power dissipated normalised by $\mathcal{P}_0 \equiv \mathcal{P}(\gamma = 0)$, $\mathcal{P}/\mathcal{P}_0$. **(b)** Detailed view of $\mathcal{P}/\mathcal{P}_0$ near $\gamma = 2/3$ **(c)** Network length, L, normalised by $L_0 \equiv L(\gamma = 0)$. **(d)** Network loop density, LD. The vertical dashed line marks the transition at $\gamma = 1/2$. Note the discontinuity of the slopes of the network's dissipation, total length and loop density.

which connects those cities [10] as depicted in Figure 5.

(a) Railway
(1384, 313, 0.45)
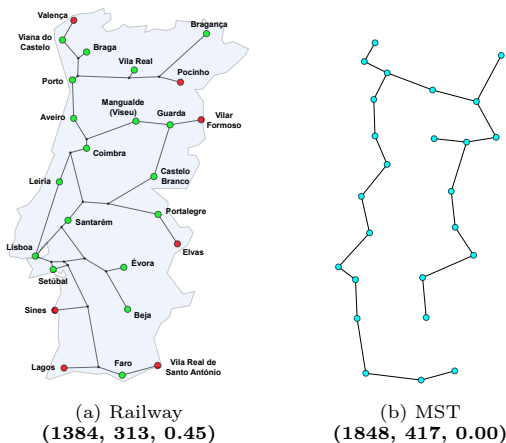
(b) MST
(1848, 417, 0.00)

FIG. 5: **(a)** Approximation of the part of the Portuguese rail network, which connects all the 18 district capitals (green nodes) and 5 additional terminal cities (red nodes). **(b)** The MST spanned by the city nodes.

The performance of the optimised networks was evaluated in terms of cost, transport efficiency and fault tolerance. The total cost of producing the network was measured by its total length (TL). The transport efficiency (TE) is defined as the inverse of the average minimum distance (MD) between all the distinct pairs of terminal cities in the final graph. Lastly, the fault tolerance (FT) is defined as the probability of the network remaining connected after a single edge is removed. Note that, as before, only the edges with conductivities above the threshold, $D_{thr} = 5 \times 10^{-4}$ are considered in the computation of the three metrics of the steady-state networks.

The final networks were also compared with the minimal spanning tree (MST) and the complete graph (CG) spanned by the city nodes. The MST is by definition the graph that connects all the city positions with minimal possible cost (TL), while the CG is the graph that connects every pair of cities by a distinct edge, maximising, therefore, the transport efficiency and the fault tolerance (FT= 1) at the expense of a tremendous cost. The cost, transport efficiency and fault tolerance of the final networks were normalised to the respective values for the CG, yielding TL_{CG}, TE_{CG}, FT_{CG}. To compare the overall performance, the trade-off between the three was captured by two benefit-cost measures, defined as the ratios $BCR_{TE}= TE_{CG}/TL_{CG}$ and $BCR_{FT}= FT_{CG}/TL_{CG}$.

Until now we have only considered the adaptation under a fixed set of sources and sinks. The previous analysis revealed that this either resulted in tree-like networks ($\gamma > 1/2$) with zero fault tolerance, or poorly-optimised networks ($\gamma < 1/2$) with large costs. Therefore, in both cases, the networks have an overall low performance, conversely to the ones built by *Physarum*. To tackle this issue, we now consider time-dependent sources and sinks. At each step of the algorithm, two nodes are randomly selected from the set of city nodes to drive the flow: one acts as a source with intensity $q_{source} = I_0$ ($I_0 > 0$) and the other as a sink $q_{sink} = -I_0$, while the remaining terminals have $q = 0$ [3]. This emulates more closely the shuttle streaming characteristic of *Physarum* networks, by changing the flow direction in each vessel over time, although not in a periodic way.

We consider that the algorithm converges when the topology of the network remains unchanged in a period of 500 iterations. In this case, a smaller time step was used, $\Delta\tau = 0.02$.

A. Dependence of the performance on γ

Numerous simulations were carried out for different values of γ, considering the same mesh, initial conditions ($D_{ij}(0) = 1$) and seed. Some examples of the different networks reached by the system are given in Figure 6. For $\gamma < 1/2$, most of the initial mesh remains and very few preferential pathways are formed, resulting in networks with a huge cost. As γ is increased the redundant paths progressively disappear, and the system slowly converges towards the MST solution (Figure 5b). The minimisation of the cost is achieved with the inevitable complete loss of the network's robustness.

The trade-off between the network's cost, transport efficiency and fault tolerance can be better quantified by
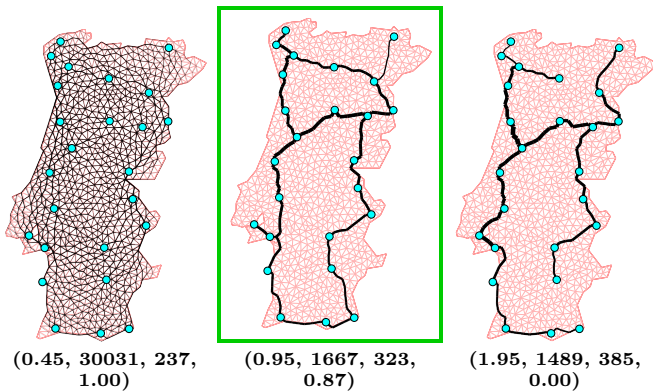
| (0.45, 30031, 237, 1.00) | (0.95, 1667, 323, 0.87) | (1.95, 1489, 385, 0.00) |

FIG. 6: Topology of the networks resulting from the adaptation dynamics (14) as a function of the parameter γ, considering a stochastic choice of the source-sink pair ($I_0 = 1$ and $D_{ij}(0) = 1$). The network with the best overall performance is highlighted in green. Labels: **(γ, TL, MD, FT)**, where TL and MD are given in kilometres.

the plots of Figure 7. As the Figures 7a and 7b confirm, the TE and FT tends to decrease as γ increases, and are always higher than the corresponding values for the MST, at the expense of a higher cost. Interestingly, most of the simulation results of the first plot lie in a well-defined curve that resembles the Pareto front [11, 12] associated with the compromise between maximising the TE while minimising the TL. The real railway is quite far from this curve. The overall performance, captured by the two benefit-cost ratios, $\mathrm{BCR_{TE}} = \mathrm{TE_{CG}}/\mathrm{TL_{CG}}$ and $\mathrm{BCR_{FT}} = \mathrm{FT_{CG}}/\mathrm{TL_{CG}}$, is depicted in Figure 7c, as a function of γ. For $\gamma \in [0.7, 1[$, the simulations result in networks with a much better compromise between the three metrics than any other graph. For higher values of γ, the networks still achieve a slightly better $\mathrm{BCR_{TE}}$ than the real railway, although the network's resilience is completely lost. In conclusion, for $\gamma \in [0.7, 1[$, the model results in networks with the overall best performance and, in general, higher than the performance of the real railway, MST and CG.

B. Dependence of the performance on the stochastic choice of terminals

We studied the impact of the method of choosing the driving terminals in each step on the topology and performance of the networks. Five different cases were studied. The first one considered was the original method proposed by Tero et al. [3] of randomly choosing in each step one source-sink pair from the set of terminals, such that $q_{source} = -q_{sink} = I_0$. This method is referred to as the "Random pair" method. In the second case ("Random source" method) , one city is randomly assigned as the source, with $q_{source} = I_0$, while all the remaining cities are sinks. The third method, ("All random") considers that the nodes' net fluxes of the terminals (q_i with $i \in T$) are time-dependent random variables subject to the constraint $\sum_{i \in \text{sources}} q_i = -\sum_{i \in \text{sinks}} q_i = I_0$. We

also compare with the case of fixed terminals, where some cities were assigned as constant sources and the others as constant sinks ("Fixed Terminals" method). All these methods were tested considering $\gamma = 2/3$ in (14). Finally, we simulated the *Physarum Solver* model [3], with the choice of a sigmoidal response typically used in literature, $f(|Q_{ij}|) = |Q_{ij}|^\gamma/(1 + |Q_{ij}|^\gamma)$, and considering the "Random pair" stochastic choice of driving terminals ("PS - random pair" method). In this case, the simulations were performed using $\gamma = 1.8$ and $I_0 = 2$, which according to [3] are the parameters that yielded networks mimicking the Tokyo rail system with the best overall performance. To establish an even comparison, the same inlet flux, I_0, was used in the other cases.

As the Figure 8 shows, different methods of choice lead to steady states with distinct topological features. Note how worse is the performance of the network produced by "Fixed Terminals" compared to the ones of stochastic methods. A more visual quantification of the performance is given by the plots of Figure 9.

The choice of fixed terminals is definitely the method that leads to networks with the worst performance by far in every respect. The simulation points are all scattered, but in every case, the performance metrics are consistently low. The characteristic tree-like topology of the steady states entails a great cost without any benefit in terms of transport efficiency, as the terminals are on average very distant from each other, and in terms of tolerance to damage, as no redundant paths are formed (FT = 0).

The results clearly show the importance of flux fluctuations in the design of low-cost, efficient and robust flow networks [3, 8, 9, 12]. All the stochastic methods resulted in networks on average much more efficient and resilient than any other network, including the railway and the MST. They also achieve better overall performance, i.e., benefit-cost relationship. Only the "Random pair" method produced networks with a slightly lower cost-efficiency compromise ($\mathrm{BCR_{TE}}$) than the railway and the MST, due to having the highest cost from all the stochastic methods. However, they achieve a far better cost-resilience trade-off.

Due to the Pareto nature of the optimisation, the criteria of choosing the best stochastic method to generate the driving terminals depends on the relevance of each metric in a given context. Assuming we want to maximise the overall trade-off between the three metrics, the results suggest that the "All Random" method is the best choice, given that is the method which achieved the highest $\mathrm{BCR_{TE}}$ and highest $\mathrm{BCR_{FT}}$ from all the tests of our model.

VII. GROWTH MODEL

So far we have only modelled the network optimisation of static organisms and neglected the continuous network formation displayed by *Physarum*. To incor-
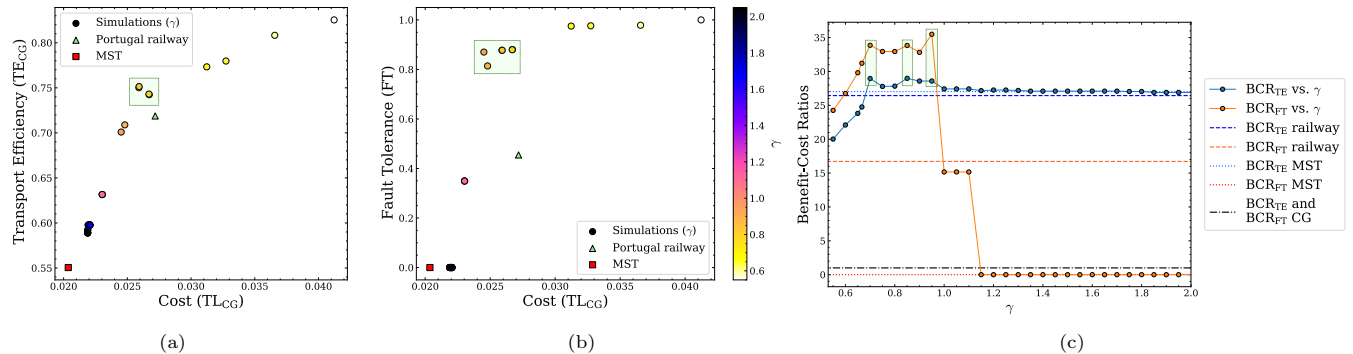
(a)

(b)

(c)

FIG. 7: Network performance of the adaptation dynamics (14) as a function of the parameter γ. **(a-b)** Transport efficiency and fault tolerance plotted against the total length of the network. The metrics are normalised to those of the complete graph (CG). The coloured circles represent the simulation results as γ was varied from 0.55 to 2.00, considering the stochastic choice of the source-sink pair The results were compared with the same metrics of the real railway (green triangles) and MST network (red squares). **(c)** Plots of the benefit-cost ratios as the function of γ, compared with the ones of the real railway, MST and CG. The proposed optimal models are highlighted in green.

(a) "Random source"
(1790, 290, 0.60)

(b) "All random"
(1714, 304, 0.91)

(c) "Fixed terminals"
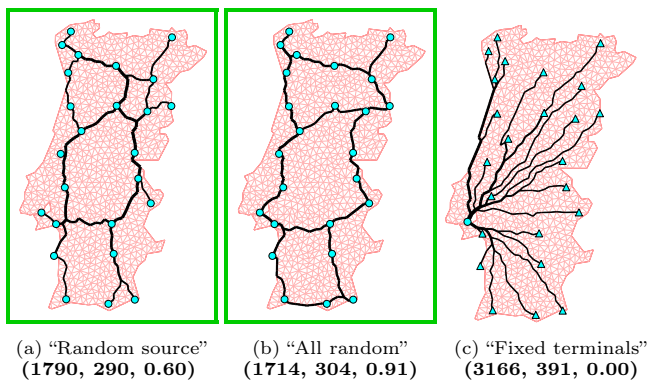**(3166, 391, 0.00)**

FIG. 8: Topology of the optimised networks considering different methods of choosing the sources and sinks in each step ($I_0 = 2$, $D_{ij}(0) = 1$). Legend: **(TL, MD, FT)**, where TL and MD are given in kilometres.

porate the growth into the previous model, *Physarum* is now represented by a dynamic graph. Growth is regarded as the formation of new channels at the boundary of the organism when there are enough nutrients in the neighbourhood to build them. The nutrients are supplied by active food sources, initially placed at certain nodes, and transported to the nodes at the boundary where they are stored until they are used in the veins' development. In this way, the boundary nodes behave like sinks of the nutrient flux, mimicking simulated regions where the growth occurs (growth fronts).

It's assumed that the dynamics take place on top of a pre-existing planar mesh. The formation of the new channels is simulated by the progressive activation of the edges of the underlying mesh when the cost of producing it is overcome. Each edge of the mesh is thus associ-

ated with a nutrient cost of activation, and can have two possible states: inactive ($D_{ij} = 0$) or active ($D_{ij} > 0$).

On the other hand, each node i is characterised by an amount of nutrients, m_i, and can be in one of three possible states. Nodes that are not yet part of the network are said to be inactive. Nodes in the growing state are located at the boundary and participate in channels formation. Active nodes are in this state as long as they contain at least one inactive neighbour node. The remaining interior active nodes are said to be in the transport state and serve only as intermediaries to transport nutrients to the boundary. In addition, any given node can have a food source, which is "activated" from the moment that the node is activated i.e., it's changed to the growing state. For simplicity, it's assumed that the food sources never run out.

A. Algorithm

The algorithm compromises three main steps which are described as follows. Initially, the *Physarum* is represented by a single node containing a food source.

In each time step, the nutrients flow from the active food sources to the current boundary sinks via the active channels, where they are accumulated. Each active source injects $q_{source} = I_0$ nutrients, which are distributed between the boundary sinks, in such a way that (3) is satisfied. Given the current sets of boundary nodes and of active food sources, the fluxes of the active channels are computed through the conservation laws (4), as described before. Then, the nutrient reserves of the boundary nodes are increased according to the flux that each receives i.e., $|q_i|$ with $i \in$ boundary. Assuming
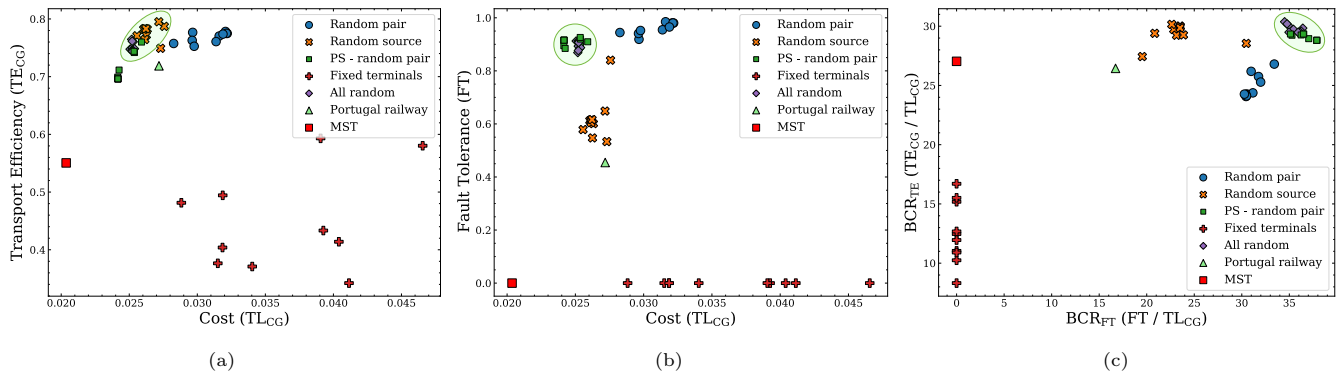
FIG. 9: Performance of the networks for different methods of choosing the sources and sinks over time.**(a-c)** Trade-off between the cost, transport efficiency and fault tolerance of the networks. Each type of marker corresponds to a different method. The networks are compared with the railway (green triangles) and MST network (red squares) **(c)** The benefit-cost ratios are plotted against each other, measuring the overall compromise between the three metrics. The optimal simulations for each trade-off are highlighted in green.

the fluid has a unitary density, the amount of nutrients that a given boundary node accumulates per time step is $dm_i = |q_i| \Delta \tau$, where $\Delta \tau$ is the duration of the time step. In the beginning, while *Physarum* is a single node covering a food source, only the last step is applied.

The next step is the network's growth. For each boundary node, it's computed the set of the incident edges which are currently inactive, i.e., edges where new channels can be formed. The nutrient reserves of the node are equally distributed among those neighbour inactive edges, and the production cost of each inactive edge is reduced by the amount of nutrients given. If the nutrients transferred to an edge exceeds its production cost, the excess is kept stored on the boundary node. When the cost of producing the channel reaches zero, the edge is activated, and a new channel is created with a conductivity $D_{ij}(0) = D_0$. If the other end node of the edge is inactive, the node is activated on the "growing state", and the boundary is extended with the new sink node. Note that every time a new channel with length L_{ij} is formed, the total network's volume, $\mathcal{V}$, is increased by $\sqrt{D_0} L_{ij}$. It's also assumed that the cost of producing a channel is proportional to its initial volume.

Finally, if all the neighbour nodes of a given boundary node are activated, the node is changed to the "transport state", and growth can no longer occur starting from it. The eventual nutrient reserves of the node are evenly distributed between the neighbours on the "growing state" which give continuity to the network growth.

Finally, the conductivities of the active channels are adapted according to the dynamics (9) for a given choice of the function g. In the following we consider the same adaptation dynamics as before (14).

B. Results

We started by analysing the simplest case of the individual growing from a food source, without any more

food sources available in the surroundings. We simulated the growth-adaption model for different values of γ, considering an even distribution of the source nutrients between the boundary sinks. Although the dynamics produced a natural isotropic growth mechanism, and the resultant networks shared some traits with real *Physarum* networks, the characteristic loopy hierarchical structure of veins couldn't be reproduced.

We then tested the hypothesis of this structure arising from fluctuating loads, by considering a random distribution of nutrients between the sinks in each step. However, we concluded that it still wasn't sufficient to explain the observed reticulated structure.

Finally, we simulated the case of *Physarum* accommodating new food sources as it grows, which is a better representation of its foraging behaviour. Since it's not clear how real organisms manage food consumption in this case, we tested two possible mechanisms, considering the growth in the presence of two food sources. In both cases, the nutrients supplied by the active food sources are evenly shared among the boundary sinks, and the simulations were performed with $\gamma = 2/3$, $I_0 = 0.1$, $D_0 = 0.1$ and $\Delta \tau = 0.02$.

In the first case, we considered that as soon as the second food source was reached, both food sources were constantly operational and injected the same amount of nutrients into the network. Snapshots of the simulation are depicted in Figure 10. As the images show, after the second food source is accommodated, the short connections between the two are weakened and ultimately collapse. This is the opposite of the true *Physarum*'s behaviour, which tends to connect the food sources through short paths to optimise the transport of nutrients and minimise the costs.

In the second case, we considered that after the second food source was activated, only one of them was operational at a time. In each time step, one of the food sources was randomly selected to supply the nutrients to the boundary nodes. The results can be found in Figure

11. The asynchronous operation of the food sources generates flow reversals which are a better approximation of the shuttle streaming behaviour of *Physarum*. Similar to what is observed in the real organism, this mechanism results in the formation of short connections between the food sources. In conclusion, the results suggest that the second mechanism is far more biologically reasonable than the first one.
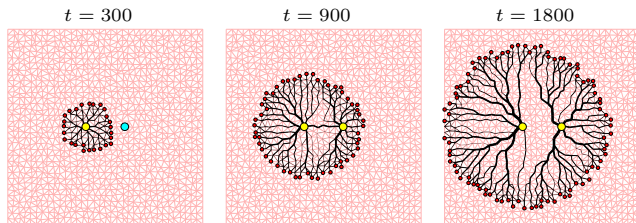

FIG. 10: *Physarum* growing in the presence of two food sources with constant input flux. The synchronous activation of both food sources leads to their "repulsion".
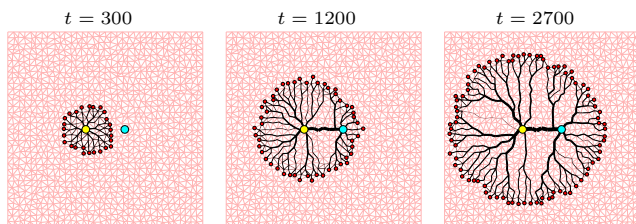

FIG. 11: *Physarum* growing in the presence of two food sources supplying nutrients alternately. The asynchronous operation of the food sources results in a short connection between them.

VIII.   CONCLUDING REMARKS

In this work, we studied the network development and adaptation of *Physarum polycephalum*. We first derived a general class of equations that correctly describes the adaptation dynamics of a network comprised of elastic channels filled with an incompressible fluid subject to a Hagen-Poiseuille flow. Then, following a Lagrangian approach, we proved that the particular choice of $g(|Q_{ij}|) = |Q_{ij}|^{2/3}$ minimises the total power dissipated by the network at the steady-state assuming a fixed set of sources and sinks. It was also observed that the same configuration of terminals could result in different steady-states depending on the initial conductivities. The analysis of the adaptation dynamics under the general class of polynomial functions, $g_\gamma(|Q_{ij}|) = |Q_{ij}|^\gamma$, revealed the existence of a first-order phase transition in the system near $\gamma = 1/2$, marked by the discontinuity of the derivative of dissipated power at the steady state with respect to γ and a drastic change in the network topology. The simulations on the arena mimicking the Portuguese mainland revealed the importance of fluctuating loads to build efficient and resilient networks. In general, all the stochastic distributions produced networks with overall better performance than any other case. Lastly, we extended the adaptation model to incorporate the network growth, coupling both processes and providing a better description of Physarum's foraging behaviour. In particular, we found that in the presence of two food sources, when they operate alternately, a strong direct connection between the two is established, similarly to what is observed in *Physarum*.

[1] K. Alim, G. Amselem, F. Peaudecerf, M. P. Brenner, A. Pringle, *Proceedings of the National Academy of Sciences* **110**, 13306 (2013).

[2] T. Nakagaki, H. Yamada, Á. Tóth, *Nature* **407**, 470 (2000).

[3] A. Tero, *et al.*, *Science* **327**, 439 (2010).

[4] A. Tero, R. Kobayashi, T. Nakagaki, *Journal of Theoretical Biology* **244**, 553 (2007).

[5] S. Bohn, M. O. Magnasco, *Phys. Rev. Lett.* **98**, 088702 (2007).

[6] J. Haskovec, L. Kreusser, P. Markowich, *Communications in Mathematical Sciences* **17**, 1235 (2019).

[7] R. P. Feynman, R. B. Leighton, M. Sands, *The Feynman lectures on physics* (1975), vol. 2, chap. 19. "Note added after the lecture".

[8] F. Corson, *Phys. Rev. Lett.* **104**, 048703 (2010).

[9] E. Katifori, G. J. Szöllősi, M. O. Magnasco, *Phys. Rev. Lett.* **104**, 048704 (2010).

[10] Portugal's railway system map, https://www.infraestruturasdeportugal.pt/pt-pt/rede. Accessed: June of 2021.

[11] R. Dilão, D. Muraro, M. Nicolau, M. Schoenauer, *Evolutionary Computation, Machine Learning and Data Mining in Bioinformatics*, C. Pizzuti, M. D. Ritchie, M. Giacobini, eds. (Springer Berlin Heidelberg, Berlin, Heidelberg, 2009), pp. 176–190.

[12] H. Ronellenfitsch, E. Katifori, *Phys. Rev. Lett.* **123**, 248101 (2019).